Conformational Pathways of Saturated Six-Membered Rings. A Static and Dynamical Density Functional Study

Andrei R. Ionescu,*,† Attila Bérces,‡ Marek Z. Zgierski,† Dennis M. Whitfield,§ and Tomoo Nukada||

Steacie Institute for Molecular Sciences, National Research Council of Canada, Theory and Computation Program, 100 Sussex Drive, Ottawa, Ontario K1A 0R6, Canada, Computational Chemistry Logic Ltd., Madach. u. 20, 8900 Zalaegerszeg, Hungary, Institute for Biological Sciences, National Research Council of Canada, 100 Sussex Drive, Ottawa, Ontario K1A 0R6, Canada, and The Institute of Physical and Chemical Research (RIKEN), Wako-shi, Saitama 351, Japan

Received: April 27, 2005; In Final Form: July 12, 2005

The conformation of the six-membered ring of pyranosyl sugars has pronounced effects on the physical and chemical properties of carbohydrates. We present a method to determine key features of the potential energy surfaces, such as transition states associated with the inversion pathways of the model compounds cyclohexane, tetrahydropyran, *p*-dioxane, *m*-dioxane, *s*-trioxane, and 2-oxanol. Finally, we make the first determination of the pathways for inversion of penta-*O*-methyl-α-D-glucopyranose and penta-*O*-methyl-*β*-D-glucopyranose. For both anomers, a transition state with five coplanar atoms with appreciable ^{O}E character was found. The method is based on constrained Car−Parrinello ab initio molecular dynamics, as implemented in the projector augmented-wave (PAW) method. The constraints are derived from the normal modes of six-membered rings and are described in terms of the canonical conformations $^{1}C_4$ chair, ^{1,4}B boat, and $^{O}S_2$ skew-boat. The PAW derived trajectories are in agreement with previous suggestions in the literature that pseudorotation is an important feature of such conformational interconversions. The dynamic nature as well as the internal coordinate-based constraints provide a method which can reliably accommodate pseudorotation. To determine semiquantitative energies, we recalculate key conformations using standard quantum mechanical calculations while keeping the ring dihedral angles frozen at their values found in the dynamics. In all cases where experimental barriers are known, our results are in excellent agreement.

1. Introduction

Ring conformation is an essential factor in the hydrolysis and the synthesis of the glycosidic bond. The mechanism of the reactions involved in the synthesis of oligosaccharides using chemical glycosylation[1] or glycosyl transferases[2−4] as well as the degradation of oligosaccharides by solvolysis reactions[5−7] or glycosidases[8] implies changes in the ring conformation. Recent atomic force microscopy experiments were interpreted as indications that polysaccharides owe their elasticity to the chair−boat flips of the pyranose ring.[9] Our previous studies of the neighboring group-assisted glycosylation reactions, by quantum chemistry calculations, revealed that, in some cases, the relative energies of pyranose conformations determine the transition states between crucial steps.[10,11] Our previous studies also suggest that chemical modification of the rigidity of the pyranose ring controls the stereochemistry and determines the product distribution.[10,12,13]

Our present goal is the complete characterization of the conformational potential energy surface of pyranoses. We believe that the mapping of the stationary points on the potential energy surface of pyranoses is a necessary prerequisite for the explanation of the biological functions of carbohydrates. Of most importance are the saddle points because experimental information concerning transition states is extremely limited. In the present paper, we developed a new method to explore the potential energy surface of pyranoses with particular emphasis on finding transition states along conformational and reaction pathways.

The application of existing algorithms of quantum chemistry to study the reaction mechanism involving the change in pyranose conformation is not straightforward. The first difficulty lies in the multitude of possible conformations. Pyranoses have 38 distinct basic conformations: 2 chairs, 6 boats, 6 skew-boats, 12 half-chairs, and 12 envelopes.[14] In addition, there are stable conformations that do not always conform with any of the 38 basic conformations.[15] New intermediate stable conformations are made possible by different substituents, attached fused rings, and double bonds; e.g, there are 24 additional conformations for 2,6-*cis*- and 2,6-*trans*-substituted dyhydropyrononones that are intermediates between envelope and half-chair conformations.[15] Even the simplest and most symmetrical saturated six-membered ring compound, cyclohexane, has stationary points which cannot be described by any of the chair, boat, skew-boat, half-chair, or envelope conformations.[16] The brute-force approach to the conformational problem of pyranoses is to optimize the geometry of all 38 basic conformations. However, because not all stationary points lie close to one of the 38 basic conformations, it is possible to miss some important conformations.

The second difficulty lies in the nature of the stationary points and the algorithms used to optimize these stationary points. The

† Steacie Institute for Molecular Sciences.
‡ Computational Chemistry Logic Ltd.
§ Institute for Biological Sciences.
|| The Institute of Physical and Chemical Research. Current address: Department of Fermentation Science, Faculty of Applied Bioscience, Tokyo University of Agriculture, Sakuragaoka, 1-1 Setagayaku, Tokyo 156-8502, Japan.

10.1021/jp052197t CCC: $30.25
Published on Web 08/17/2005

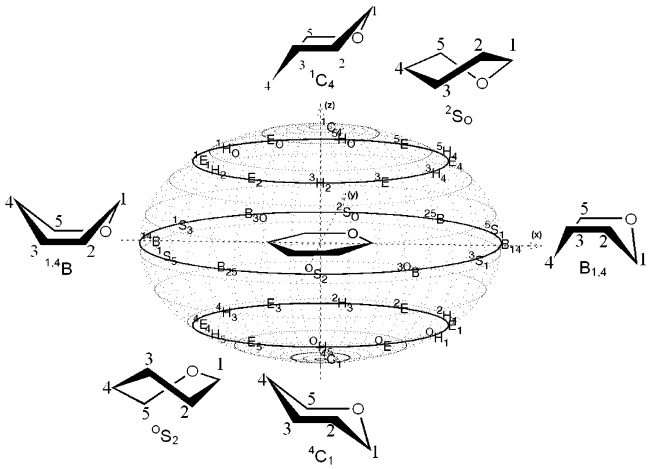

Figure 1. Spherical mapping of pyranose conformations.

chair and skew-boat conformations are usually minimal, the boat and half-chair conformations are first-order transition states, the envelope conformations are second-order transition states, and there are several exceptions from these rules.

It is not possible to tell a priori the nature of each conformation; furthermore, different algorithms need to be used to optimize stable structures or transition states. It is particularly difficult to find transition states on the ring conformational potential surface because of the nature of the eigenvectors involved in the conformational transitions. Transition-state (TS) optimization methods rely on identifying the eigenvector corresponding to the reaction coordinate. Conformational transitions of six-membered rings involve the continuous mixing of two or three eigenvectors. For this reason, the straightforward application of TS optimization algorithms is often unsuccessful. To explore the potential energy surface of ring conformational transition, it was necessary to develop new methods that take into account the physical nature of the conformational degrees of freedom and the possible pathways of converting one conformation into another.

2. Conformational Constraints

The conformational analysis of the potential energy surface of six-membered pyranose rings by quantum chemistry methods requires that the geometry can be constrained to any particular conformation during optimization. The conformational degrees of freedom of the six-membered rings arise from the three out-of-plane normal modes of the regular hexagon. These three normal modes correspond to the distortion of the planar ring into chair, boat, and skew-boat conformations. All pyranose ring conformations can be uniquely described in terms of one chair, one boat, and one skew-boat conformation, but it proves convenient to use the $^1C_4$ chair, $^{1,4}B$ boat, and $^{O}S_2$ skew-boat conformations, which we call canonical conformations.[17] If distortions into $^1C_4$ chair, $^{1,4}B$ boat, and $^{O}S_2$ skew-boat conformations are represented by points on the *z*, *x*, and *y* axes of an orthogonal coordinates system, respectively, all boat and skew-boat conformations derived by permutation of the atom numbering lie on a circle in the *xy* plane. The half-chair and envelope conformations lie on a smaller radius circle between the *xy* plane and the chair coordinate on the *z* axis. Thus, as originally suggested by Hendrickson, all pyranose ring conformations are conveniently represented on a sphere and characterized by spherical polar coordinates (Figure 1).[18] The radius is the puckering amplitude, and the angular coordinates determine the type of conformation. There have been several proposals for the mathematical expression of the spherical polar coordinates, including our own definition.[17] The most popular definition was introduced by Cremer and Pople (CP) who expressed the ring conformation as a function of the Cartesian atomic coordinates.[19] Alternatively, spherical polar coordinates can be derived by Fourier transform from the ring torsion angles.[20,21]

In the preceding paper,[17] we have derived quantitative expressions for the characterization of the pyranose and other six-membered ring conformations which rely heavily on the definitions of the natural internal coordinates introduced by Pulay et al.[22,23] If τ_1, τ_2, τ_3, τ_4, τ_5, and τ_6 torsion angles are defined by the $C_1C_2C_3C_4$, $C_2C_3C_4C_5$, $C_3C_4C_5O$, $C_4C_5OC_1$, $C_5OC_1C_2$, and $OC_1C_2C_3$ atom sets, respectively, displacement into the $^1C_4$ chair conformation is described by the

$$q_1 = \tau_1 - \tau_2 + \tau_3 - \tau_4 + \tau_5 - \tau_6 \tag{1}$$

internal coordinate. Displacement into $^{1,4}B$ boat (q_2) and $^{O}S_2$ skew-boat (q_3) conformations are described by the internal coordinates

$$q_2 = \tau_2 - \tau_3 + \tau_5 - \tau_6 \tag{2}$$

$$q_3 = \tau_1 - \frac{1}{2}\tau_2 - \frac{1}{2}\tau_3 + \tau_4 - \frac{1}{2}\tau_5 - \frac{1}{2}\tau_6 \tag{3}$$

respectively.

The phase angle of pseudorotation can be defined as a function of q_2 and q_3 internal coordinates:

$$\phi = \arctan\left(\frac{\sqrt{3}q_2}{2q_3}\right) \tag{4}$$

The $\sqrt{3}/2$ term arises from normalization factors. Equation 4 is consistent with the Cremer−Pople definition of ϕ, provided that the ring atoms are numbered by carbohydrate numbering. In that case, the zero value of the phase angle, ϕ, corresponds to the $^{1,4}B$ boat conformation.

The internal coordinates defined in eqs 1−3 can be applied as constraints. Although they may not be the most suitable constraints, their availability in quantum chemistry programs makes them an attractive choice. For example, the transformation from $^{O}S_2$ to $^{2}S_O$ conformations can be studied with q_3 of eq 3 as a constraint. The midpoint of the pseudorotational circle (Figure 1) corresponds to the planar conformation, and the radius determines the amplitude of displacement from the planar conformation into the $^{O}S_2$ conformation. However, any other conformation (in this case, any other twistboat) can be described by the internal coordinate q_3 by permutation of atom numbers in the definition of the internal coordinate. For example, starting the atom numbering with C_2 instead of C_1 in the definition of the q_3, we can describe distortion into the $^1S_3$ conformation. Opposite conformations correspond to the same internal coordinate with the opposite sign. By increasing the value of q_3 from a negative to a positive value, one may induce a conformational change that turns the $^{O}S_2$ into the $^{2}S_O$ conformation. By allowing the complementary internal coordinates to evolve according to the lowest-energy path, the reaction follows the pseudorotational itinerary instead of going through the energetically forbidden planar conformation. The drawback of using constraints such as q_2 and q_3 is that there is no control over whether the transition follows a clockwise or counterclockwise transformation along the pseudorotational itinerary. The direction will be determined by the lower energy of distortion at the starting conformation. However, this direction does not necessarily correspond to the

overall lowest-energy reaction pathway because the potential may sharply increase at a subsequent conformation. Another drawback of such constraints is that they do not have high projection onto the intrinsic reaction coordinate (IRC) throughout the reaction. This is a requirement for the calculation of thermodynamic properties along the reaction pathway by constrained reaction dynamics. We used q_1 to explore the chair inversion process and q_2 and q_3 to explore the pseudorotational itinerary.

3. Computational Details

3.1. Dynamical DFT Calculations. Dynamical density funtional theory (DFT) calculations were carried out with the projector augmented-wave (PAW) method of Blöchl,[24] which is an implementation of the Car−Parrinello ab initio molecular dynamics.[25] The energy cutoff of the plane wave basis set was set to 30 Ry, and the calculations used the frozen-core approximation. All calculations employed the exchange correlation functional of the generalized gradient approximation with the local potential of Perdew and Zunger[26] augmented by the gradient corrections to the exchange and correlation of Becke and Perdew. Periodic boundary conditions were used with a unit cell defined by lattice vectors ([0.0 10.0 10.0] [10.0 0.0 10.0] [10.0 10.0 0.0]) Å for the test molecules and by lattice vectors ([0.0 14.0 14.0] [14.0 0.0 14.0] [14.0 14.0 0.0]) Å for D-glucopyranose. To prevent electrostatic interactions between periodic images, a charge-isolation scheme was used.[27] A temperature of 300 K was maintained for all simulations by a Nosé thermostat.[28,29] The fictitious kinetic energy of the electrons was controlled in a similar fashion by a Nosé thermostat.[30] To span large portions of configuration space in a minimum amount of time, the true masses of the nuclei were rescaled to 3.0 (O and C) and 1.5 (H) atomic mass units. Together with an integration step of 7 au (0.17 fs), this choice ensures good energy conservation during dynamics simulations without computational overhead due to heavy atomic nuclei. Because we do not discuss time-dependent properties and because configurational ensemble averages remain unchanged under a rescaling of the masses, this technique is appropriate. To sample space in the vicinity of the transition state, we chose a reaction coordinate (RC) which was kept constrained during the dynamics with the SHAKE algorithm.[31] All other degrees of freedom are allowed to evolve naturally in time. By slowly varying the constraint, we can sample phase space in the vicinity of the transition state dynamically, leading to undisturbed dynamics for all motions which are orthogonal to the RC and to the fictitious dynamics along the RC. All simulations consisted of 70 000 (test molecules) and 90 000 time steps which cover 11.9 and 15.3 ps real time, respectively, unless otherwise indicated in the text.

The free-energy difference, ΔF, between two arbitrary points (λ_1 and λ_0) along the reaction coordinate can be evaluated by integrating the average force on λ at a given constant temperature, T:

$$\Delta F = F(\lambda_1) - F(\lambda_0) = \int_{\lambda_0}^{\lambda_1} \left\langle \frac{\delta E}{\delta \lambda} \right\rangle_{\lambda} \mathrm{d}\lambda \qquad (5)$$

The reaction coordinate can be sampled with discrete values of λ or allowed to vary continuously in what is called a *slow-growth* simulation. In the latter method, the system is never properly equilibrated unless the change in the RC is infinitesimally small. The *slow-growth* method has been previously demonstrated on several elementary reactions steps in organometallic chemistry.[32−35] In the *slow-growth* method, the energy gradient is not averaged at constant values of λ, therefore it does not yield the free energy exactly. However, this method is successful for the qualitative understanding of the reaction mechanism, the location of stationary points on the free-energy surface, and the semiquantitative calculation of free-energy differences.

TABLE 1: Barriers to Chair to Skew-Boat Conversion in kJ·mol^{-1} at 300 K[a]

compd	ΔH (calcd)[b]	ΔH (exptl)[c]	ΔG (calcd)[b]	ΔG (calcd)[d]	ΔG (exptl)[e]
cyclohexane	43.5	38.0−48.0	48.0	41.4	∼43
tetrahydropyran	42.6	42.0 ± 5.0	41.8	39.7	41.0 ± 1.6
m-dioxane	41.8	40.0 ± 2.1	40.5	40.1	41.0 ± 0.8
p-dioxane	43.0	na	42.6	41.0	∼41
s-trioxane	41.8	37.0 ± 5.0	35.5	48.5	46.0 ± 0.8

[a] See Figure 2 for canonical conformations. [b] Fully optimized at the b3p86/6-311+g** level. [c] See ref 41. [d] Calculations were carried out with PAW. [e] See ref 42.

TABLE 2: Barriers to Skew-Boat to Chair Conversion in kJ·mol^{-1} at 300 K[a]

compd	ΔH (calcd)[b]	ΔH (exptl)	ΔG (calcd)[b]	ΔG (calcd)[c]	ΔG (exptl)[d]
cyclohexane	17.1	na	23.8	18.0	22.5 ± 0.2
tetrahydropyran	18.4	na	19.6	16.7	na
m-dioxane	16.3	na	17.6	23.4	na
p-dioxane	15.5	na	17.6	15.0	na
s-trioxane	20.5	na	16.7	23.8	na

[a] See Figure 2 for canonical conformations. [b] Fully optimized at the b3p86/6-311+g** level. [c] Calculations were carried out with PAW. [d] See ref 43.

3.2. Static DFT Calculations. The reported static calculations were carried out with the Gaussian 98 program package.[36] All optimized static geometries calculated in this study are based on the generalized gradient approximation (GGA). All calculations were performed with the B3P86 method combining Becke's 3-parameter exchange functional[37] with the Perdew 86 correlation functional.[38,39] The basis set was 6-311+G**. Full geometry optimization followed by complete frequency analysis was performed in all cases.

4. Results and Discussion

Thermodynamical experimentally measured data on saturated six-membered rings consist of values for the energy barriers of the chair inversion and the skew-boat to chair isomerization as well as values for the rate of inversion of the rings. First, we investigated the conformational potential energy surface of cyclohexane, tetrahydropyran, *m*-dioxane, *p*-dioxane, and *s*-trioxane to test various aspects of the constrained dynamics, such as the different constraints, the energy conservation, and the numerical accuracy by two-way simulations. Secondly, we investigated the simplest model for the pyranose ring (2-oxanol) to further test our constrained method and to compare our results with previous high-level theoretical calculations. Finally, we investigated the complete conformational potential energy surface of D-glucopyranose.

4.1. Benchmark Applications and Tests. Tables 1 and 2 show the experimentally determined free energy and enthalpy of activation of cyclohexane and its derivatives vs our calculated values. The free-energy values were computed by dynamical simulations at 300 K with eq 5 and by static DFT simulations. The enthalpy of activation values were obtained by static DFT thermochemistry calculations at 300 K.

The calculated-energy and free-energy barriers for chair to skew-boat conversion, listed in Table 1, are in excellent

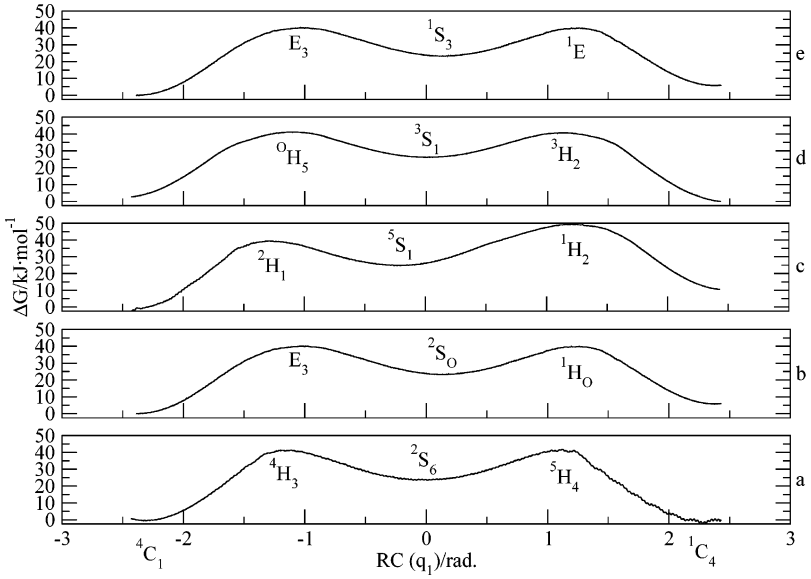

Figure 2. Free-energy diagrams in kJ·mol^{-1} for the inversion of saturated six-membered rings: (a) cyclohexane, (b) tetrahydropyran, (c) *m*-dioxane, (d) *p*-dioxane, and (e) *s*-trioxane.

agreement with the experimental values[40,41] and are within the numerical accuracy of the calculations of the experimental error range.

The calculated-energy and free-energy barriers to skew-boat to chair conversion are listed in Table 2. Experimental values, at room temperature and in gas phase, corresponding to our simulations are not available. The only experimental value for the free-energy barrier of cyclohexane skew-boat−chair isomerization was measured at 100 K in an Ar matrix.[42]

Next, we discuss the conformational interconversion of the different six-membered ring compounds on the basis of dynamical and static DFT calculations.

4.1.1. Cyclohexane. Figure 2a shows the free-energy diagram corresponding to the inversion of cyclohexane using the q_1 constraint. The dynamical trajectory obtained by constraining the cyclohexane inversion using the q_1 chair coordinate involves two half-chair transition states ($^5H_4$ and $^4H_3$) and a skew-boat ($^2S_6$) secondary minimum. The free-energy diagram is symmetric with both chair to skew-boat barriers of 41.4 kJ·mol^{-1}. The first transition state ($^5H_4$) normally connects the chair ($^1C_4$) conformation to the skew-boat ($^5S_1$). The fact that the secondary minimum is the $^2S_6$ skew-boat suggests that the transition state pseudorotates. This confirms the conclusion of previous ab initio, semiempirical, and molecular mechanics studies that the flat nature of the potential surface around the half-chair conformation gives rise to a fluxional, pseudorotating transition state.

The second half of the trajectory follows the minimum energy pathway by connecting the $^2S_6$ skew-boat with the $^4C_1$ chair conformation through a $^4H_3$ half-chair transition state. In this case, there is also a strong contribution from pseudorotation. The energy barrier to the skew-boat secondary minimum to the chair conformations of 18.0 kJ·mol^{-1} was in good agreement with the experimental values. The static calculation free-energy and enthalpy of activation are shown in Tables 1 and 2.

Figure 3 shows the free-energy diagrams corresponding to the inversion of cyclohexane using the q_2 and q_3 constraints. The dynamical trajectories obtained using the q_2 boat and q_3 skew-boat coordinates show that, in both cases, the trajectory is constrained to the pseudorotational itinerary. The skew-boat minimum conformers along the pseudorotational circle are interconverted via boat transition-state conformations. The free-energy barriers are below 4.18 kJ·mol^{-1}, in very good agreement

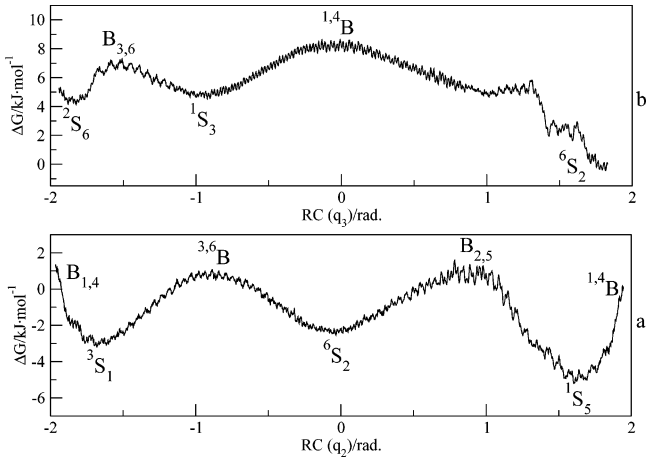

Figure 3. Free-energy diagrams in kJ·mol^{-1} for the inversion of cyclohexane using (a) the q_2 constraint and (b) the q_3 constraint.

with experimental data that found a barrier of interconversion of 3.8 kJ·mol^{-1}.

4.1.2. Tetrahydropyran. Figure 2b shows the free-energy diagram corresponding to the inversion of tetrahydropyran using the q_1 chair constraint. The three minima correspond to the two chair conformers ($^1C_4$ and $^4C_1$) and to the skew-boat stable secondary minimum (^2S_O). The free-energy barriers from $^1C_4$ to ^2S_O and from $^4C_1$ to ^2S_O are 33.9 and 39.7 kJ·mol^{-1}, respectively. The dynamical trajectory of the tetrahydropyran chair inversion does not follow the lowest skew-boat conformation and passes through an E_3 envelope transition state, which is essentially isoenergetic with the ^1H_O conformation. The free-energy barriers to the skew-boat to two chair conformations are 16.3 and 16.7 kJ·mol^{-1}. The static calculation results are shown in Tables 1 and 2 and are in good agreement with the experimental results.

4.1.3. m-Dioxane. Figure 2c shows the free-energy diagram corresponding to the inversion of *m*-dioxane using the q_1 chair constraint. The low symmetry of *m*-dioxane is well represented by the asymmetric free-energy diagram. The dynamical calculations found that the $^4C_1$ conformer is 10.0 kJ·mol^{-1} more stable than the $^1C_4$ conformer. The dynamical trajectory starts from the $^4C_1$ conformer and then passes through a $^2H_1$ half-chair transition state (the free-energy barrier is 40.1 kJ·mol^{-1}; see

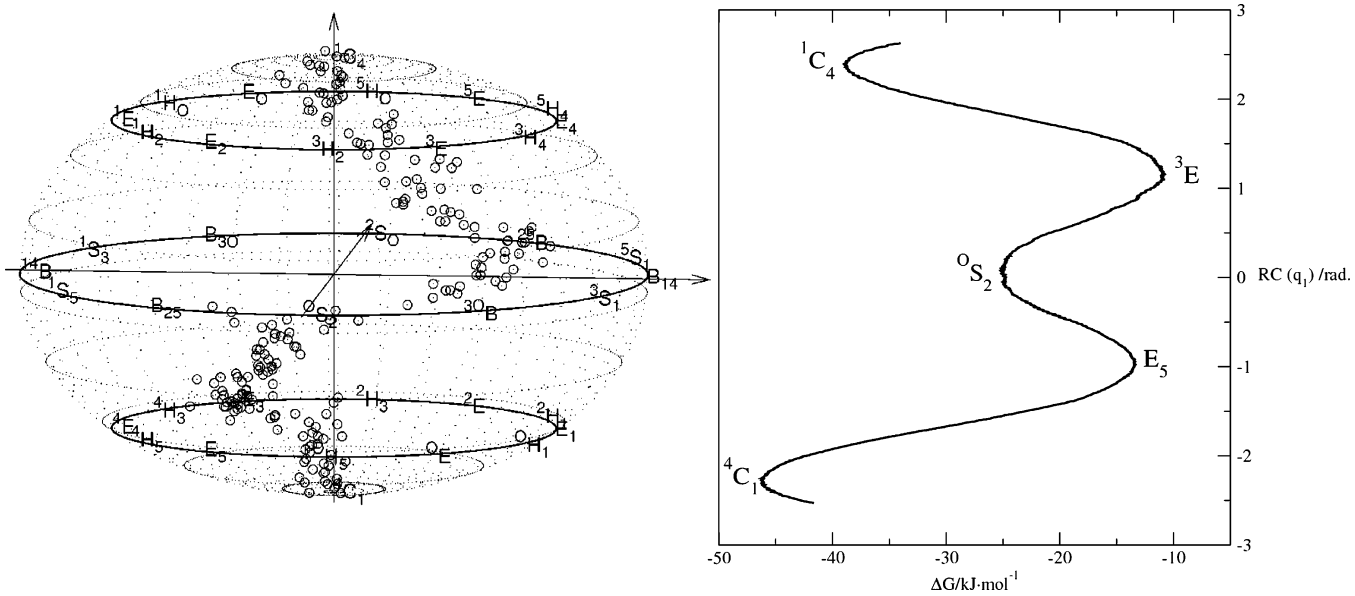

Figure 4. Free-energy curve and dynamical trajectory on the conformational sphere for the inversion of 2-oxanol.

Table 1) which leads to a $^5S_1$ secondary minimum. Interestingly, from the $^5S_1$, the trajectory follows the pseudorotational itinerary and passes through the $^1S_5$ skew-boat and then through the $^1H_2$ transition state to finally get to the inverted $^1C_4$ chair conformer. The detour on the pseudorotational circle costs an additional 9.6 kJ·mol^{-1}, and the overall free-energy barrier is 23.4 kJ·mol^{-1}.

4.1.4. p-Dioxane. Figure 2d shows the free-energy diagram corresponding to the inversion of *p*-dioxane using the q_1 chair constraint. The dynamical trajectory for the inversion of $^1C_4$ to $^4C_1$ passed through the $^3S_1$ secondary minimum. The minima were connected by $^3H_2$ and $^OH_5$ half-chair transition states. The free-energy barrier to the chair to skew-boat reaction was 41.0 kJ·mol^{-1} (Table 1), and the barrier to the skew-boat to chair reaction was 15.0 kJ·mol^{-1} (Table 2).

4.1.5. s-Trioxane. Figure 2e shows the free-energy diagram corresponding to the inversion of *s*-trioxane using the q_1 chair constraint. *s*-Trioxane inverts through two envelope transition states (^1E and E_3). The secondary minimum on the free-energy plot is a skew-boat conformer ($^1S_3$). The free-energy barrier to the chair inversion is 48.5 kJ·mol^{-1} (Table 1), and the barrier to the skew-boat to chair interconversion is 23.8 kJ·mol^{-1} (Table 2).

4.2. Pyranose Systems and Models. The simplest model for the pyranose ring is 2-oxanol. Previous studies of 2-oxanol have shown that many aspects of the hydrolysis of the glycosidic bond can be interpreted using 2-oxanol as a model system.[7,43] Our results showed that the dynamical calculations are in good agreement with previous high-level theoretical calculations and, furthermore, provided a unique insight into the chair inversion process. The next example in this section is the study of D-glucopyranose.

4.2.1. 2-Oxanol. Smith[7] has studied the conformational requirements of the hydrolysis of the glycosidic bond using 2-oxanol by very high-level (G2 theory) ab initio calculations. The relevant conformations in his study were selected on the basis of their significance in enzymatic cleavage of the glycosidic bond. Smith's study suggested that the inversion of 2-oxanol from the $^1C_4$ conformation passes through the $^3H_4$ transition state and arrives at the $^3S_1$ conformation on the pseudorotational itinerary. The $^3H_4$ transition state connects the $^1C_4$ and the $^3S_1$ conformations on the conformational map (Figure 1). Our constrained dynamical analysis found a different inversion pathway. Starting from $^1C_4$ conformation (Figure 4), the lowest-energy trajectory passed through the ^3E envelope conformation; then, the trajectory involved an evolution in the direction of the $^{3,O}B$ conformer, coupled with pseudorotation, and arrived at the $^OS_2$ conformation as the secondary minimum. This was unexpected because the $^OS_2$ conformation is connected with the $^1C_4$ conformation through the $^3H_2$ half-chair transition state. However, the ^3E envelope and the $^3H_2$ half-chair are adjacent structures and are very close in energy. From the $^OS_2$ conformation, the dynamical trajectory involved evolution that passed through the E_5 envelope conformation and arrived at the inverted $^4C_1$ chair. We have calculated the total energies of various conformations of 2-oxanol and confirmed that there is a strong preference for the $^OS_2$ conformation with respect to the $^3S_1$ conformation. The relevant thermodynamic data are summarized in Table 3. For those conformations characterized by Smith,[7] the relative energies qualitatively agree between the QCI/631-G(d) and the present DFT calculations.

TABLE 3: Energetics for 2-Oxanol in kJ·mol^{-1}

compd	*G* (calcd)[a]	*G* (calcd)[b]	*G* (calcd)[c]	*E* (calcd)[b]	*E* (calcd)[c]
$^1C_4$	0.0	0.0	0.0	0.0	0.0
$^3H_4$	30.9(^3E)	30.8	23.7	28.5	35.6
$^OS_2$	11.3	11.1	na	9.1	na
$^{3,O}B$	18.5	18.8	na	16.1	na
$^3S_1$	16.9	15.0	6.9	15.5	13.7
$B_{1,4}$	na	na	14.3	na	20.2
$^5S_1$	10.8	14.5	5.9	14.3	14.3
^2S_O	13.8	17.5	na	20.2	na
$B_{3,O}$	16.4	24.2	na	22.8	na
$^1S_3$	13.7	19.5	na	21.1	na

[a] Calculations were carried out with PAW. [b] Fully optimized at the b3p86/6-311+g** level. [c] See ref 7.

The dynamical trajectory of 2-oxanol inversion clearly showed that our dynamical approach provided a unique insight into the chair inversion process. The reaction paths suggested by the previous study and the dynamical calculations are different. The dynamical calculation showed a complex evolution: once the reaction path passed the barrier, the chair inversion was combined with significant pseudorotation. The oscillation of the pseudorotational angle around the skew-boat

conformation had a much larger amplitude than that from around the transition states, which suggested a flat potential surface around the $^{O}S_2$ secondary minimum.

4.2.2. Glucopyranose. Our main interest was the study of the inversion of α- and *β*-D-glucopyranose. D-Glucopyranose plays an essential role in biochemistry, and its structure and conformational behavior were intensively studied by theoretical means. There are more than 700 possible conformers based on the different orientations of hydroxyl and hydroxymethyl groups.[44] It has been found that both anomers, α- and *β*-D-glucopyranose, exist predominantly as $^4C_1$ conformers. Experimentally, the separation energy between the two chair conformers was 46.0 kJ·mol^{-1}.[45] Theoretical calculations ranging from semiempirical[46−49] and molecular mechanics[50−52] to ab initio,[53−57] Monte Carlo,[58−60] and molecular dynamics[61−63] have thoroughly investigated the conformational modifications of glucose rings. However, many of these calculations are based on force fields unsuitable to predict correctly the conformational potential surface of pyranoses. Ab initio calculations found, in vacuo, that the $^4C_1$ chair is about 33.4 kJ·mol^{-1} more stable than the inverted $^1C_4$. On average, the α anomer is about 1.7 kJ·mol^{-1} more stable than the *β* anomer. Previous ab initio calculations of chair−boat conversions in pyranose monomers have shown transition-energy barriers of approximately 58.5 kJ·mol^{-1}.[64] Many recent studies have concentrated on the study of solvation effects and were based on continuum models. The relative stability changes in aqueous solution, where the population of *β* anomers is lower in free energy than that of α anomers by 1.2 kJ·mol^{-1}. Previous ab initio and nanosecond molecular dynamics studies of solvated disaccharides[65] revealed a competition between the intermolecular water−maltose and intramolecular hydrogen bonds of comparable strengths in maltose, which leads to water-promoting rotation around the glycosidic bond. Atomic force microscope (AFM) manipulations of polyglucose molecules were a different and unique way of inducing conformational transitions by ellastical deformation of the pyranoid ring.[9,66]

For our studies, we chose per-*O*-methyl substitution for two reasons: First, the absence of hydroxyls prevents intramolecular hydrogen bonding. Conformations with intramolecular hydrogen bonding are found to be the lowest-energy ones by gas-phase calculations of neutral monosaccharides, and this factor may obscure other factors influencing reactivity.[67] Secondly, methyl is the smallest possible protecting group and begins to address the important issue of the effect of protecting groups on reactivity. In all cases examined so far, the preferred CH−OCH$_3$ rotamers have a lone pair anti to the sugar methine and to the methyl carbon syn to the methine (Figure 8). This conformational preference has been observed before in calculated structures of permethylated disaccharides.[68] This syn preference has been found for 2,6-disubstituted-1-methoxycyclohexanes and was ascribed to steric effects.[69]

The trajectory that we found to be the minimum energy path between the two chair conformers was determined by constrained ab initio molecular dynamics and was plotted on the conformational sphere using the Cremer−Pople parameters in Figure 5. The trajectories show that the inversion process is a mix of several modes, with a large contribution from pseudorotation.

For the penta-*O*-methyl α anomer, the MD trajectory followed a complex pathway on the potential energy surface and, in addition to inversion, it also involved pseudorotation (Figure 5). The barrier to pass to get out of the $^1C_4$ chair minimum was 10.3 kJ·mol^{-1} and involved a transition state between the ^1E envelope and ^1H_O half-chair, with the major contribution from the envelope conformation. From this point, the trajectory continued toward the $^1S_5$ skew-boat minimum and, without reaching it completely, pseudorotated and passed subsequently through the $B_{2,5}$ boat and $^{O}S_2$ skew-boat conformations. Once the conformation settled to the $^{O}S_2$ skew-boat minimum, the pseudorotation ended, and by passing through the $^{O}H_5$ half-chair as a second transition state, the inversion process ended with the $^4C_1$ inverted chair. The free-energy barrier from the $^4C_1$ chair to the $^{O}S_2$ skew-boat was 20.5 kJ·mol^{-1}, twice the free-energy barrier required to leave the $^1C_4$ chair minimum. This is consistent with experimental data that evidenced the greater stability of the $^4C_1$ chair compared to that of the $^1C_4$ chair.

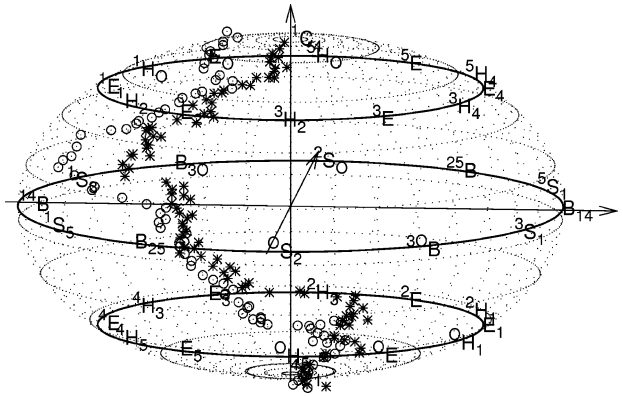

Figure 5. Dynamical trajectory on the conformational sphere for the inversion of penta-*O*-methyl-α-D-glucopyranose (circles) and penta-*O*-methyl-*β*-D-glucopyranose (stars).

For the penta-*O*-methyl *β* anomer, the MD trajectory had some significant differences from the one found for the α anomer (Figure 5). First, the transition state from the $^1C_4$ chair was a purely ^1E envelope conformation. Consequently, from the envelope-like transition state, the system evolved into the $^{1,4}B$ minimum. The barrier for this conversion was only 2.1 kJ·mol^{-1}. Secondly, the pseudorotation was around the $^1S_5$ skew-boat minimum and stopped without reaching the $^{O}S_2$ skew-boat. Thirdly, the transition state to the inverted $^4C_1$ chair was a mix of envelope and half-chair conformations. The free-energy barrier to leave the $^4C_1$ chair minimum was 7.2 kJ·mol^{-1}, nearly twice the free-energy barrier required to leave the $^1C_4$ chair minimum.

Figure 6 shows the evolution of the O1−O4 distance for the two anomers with time. For the α-D-glucopyranose anomer, the transition from chair to boat conformations increased the distance between the glycosidic oxygen O1 and the oxygen O4. For the *β*-D-glucopyranose anomer, the transition from chair to boat conformations decreased the distance between the two oxygens. These results are in good agreement with AFM studies on amylose, dextran, and cellulose[9] that found a similar variation of the length of the monomer with the pyranose ring conformation.

Constrained ab initio molecular dynamics can help qualitatively describe the conformational path, but free energies are not reliable, especially when two different modes dominate a major part of the trajectory. We have conducted a series of static calculations in which we have taken snapshots of the conformations along the MD trajectory at regular spaced intervals. Figure 7 shows the potential energy curves obtained by static calculations. The energy vs constraint plots were calculated by optimizing geometries taken from both α and *β* anomer MD trajectories, with ring dihedrals kept frozen during the optimiza-

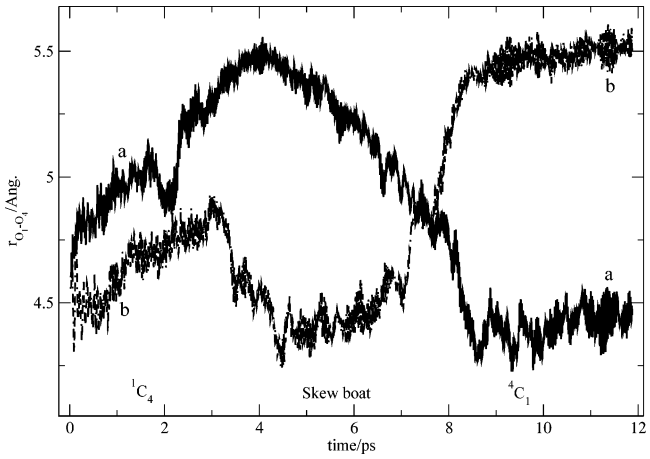

Figure 6. Time evolution of the distance O1−O4 (in Å) for (a) penta-*O*-methyl-α-D-glucopyranose and (b) penta-*O*-methyl-*β*-D-glucopyranose.

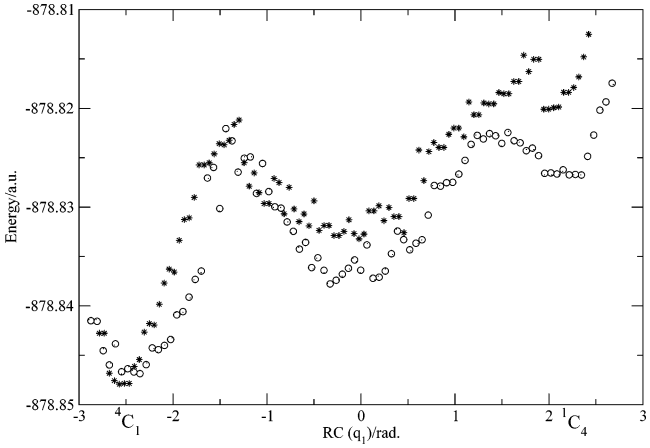

Figure 7. Static DFT pathway for the transition from the $^4C_1$ chair to the $^1C_4$ chair of penta-*O*-methyl-α-D-glucopyranose (circles) and penta-*O*-methyl-*β*-D-glucopyranose (stars).

TABLE 4: Energy Barriers for Penta-*O*-methyl-α- and Penta-*O*-methyl-*β*-D-glucopyranose Chair to Skew-Boat Conversions in kJ·mol^{-1} at 300 K

compd	ΔG (calcd)[a]	ΔG (calcd)[b]	ΔH (calcd)[b]	ΔE (calcd)[b,c]	ΔE (calcd)[d]
		$^4C_1$ to Skew-Boat			
α[e]	20.5	51.9	42.6	45.9	65.6
β[f]	7.2	37.3	30.7	33.5	70.9
		$^1C_4$ to Skew-Boat			
α[e]	10.3	na	na	na	10.5
β[f]	2.1	na	na	na	13.1

[a] Calculations were carried out with PAW. [b] Fully optimized at the b3p86/6-311+g** level. [c] ZPE included. [d] Ring dihedrals are frozen; see Figure 7. [e] Penta-*O*-methyl-α-D-glucopyranose. [f] Penta-*O*-methyl-*β*-D-glucopyranose.

tion. The rest of the molecule was allowed to optimize. This permitted us to simulate the dynamical trajectory and to calculate the thermodynamic values associated with the inversion path. Free-energy barriers obtained by both dynamic and static calculations are shown in Table 4. The $^4C_1$ chair conformation was the most stable for both α and *β* anomers. An energy plateau was found around the value zero for the constraint and corresponds to the conformations close to the pseudorotational itinerary. The $^1C_4$ chair was the less-stable conformation. The activation barriers for leaving the $^4C_1$ chair minimum for α and *β* anomers had almost equal values. However, once the transition state was passed, the trajectories followed different energetic pathways, with the *β* trajectory higher in energy than the α trajectory.

Stationary points were calculated by fully optimizing candidate structures taken from the static calculation simulated trajectory for each anomer. For the $^4C_1$ chair, we found that the *β* conformer was 1.0 kJ·mol^{-1} more stable than the α conformer. Our static calculations showed that the $^1C_4$ chair conformations were unstable. Consequently, we calculated only the transitions from the $^4C_1$ chair to the skew-boat and boat secondary minima. Next, we compared the geometries of the two anomers obtained by optimization of the candidate structures taken from the static potential energy curve. The geometrical parameters that we investigated were the C1−O5 and C1−O1 bonds and the dihedral angle O6−C5−C6−O6. The C1−O5 bond distances for α and *β* chair minima (Figure 8a,b) were 1.421 and 1.422 Å, respectively. The C1−O1 bonds are longer in α than in *β* by 0.011 Å. The O6−C5−C6−O6 dihedral angles (−71.2° for both chair anomers) showed that the two conformers are in the g conformation that some experimental NMR studies have shown to be the most populated. The O1−O4 distance is 1.041 Å shorter in the α chair anomer than in its *β* counterpart.

The investigation of the same geometrical parameters of the transition states (Figure 8c,d) showed that the C1−O bond was 0.021 Å longer in α than in *β*. Although there was no difference in C1−O1 bonds between anomers, the O1−O4 distance in the α anomer was 0.967 Å shorter than that in the *β* anomer. For the two transition states, the C1−C2−C3−C4 and C2−C3−C4−C5 ring dihedrals were 4.8° for α and 17.8° for *β* and 0.2° for α and −11.6° for *β*, respectively. The five contiguous coplanar carbon atoms suggested that, in both cases, the transition followed the route to the skew-boat conformation via an envelope saddle point. Conformation analysis pointed out that both transition structures were of ^OE envelope type. This conformation is adjacent to the $^OH_5$ half-chair transition state predicted by the MD trajectory. An attentive look at the MD trajectory revealed oscillations between the $^OH_5$ half-chair and the ^OE envelope conformations. However, the maximum energy was reached for the half-chair conformation, thus explaining our choice for the MD transition state.

The secondary minima were found to be the $^OS_2$ skew-boat for the α-D-glucopyranose and a mix of $^OS_2$ skew-boat and $^{1,4}B$ boat for the *β*-D-glucopyranose (see Table 5 and Figure 8). Although the C1−O5 and C1−O1 bonds have similar values, the O1−O4 distance is 0.699 Å larger in the α than in the *β* anomer.

For the α anomer, the transition from chair to skew-boat increased the O1−O4 distance by 0.640 Å and the remaining selected geometrical parameters did not suffer a significant change. The calculated increase is 12.3%, and the experimental measured values are 16.8 ± 1.8% for amylose and 19.5 ± 2.1% for dextran. For the *β* anomer, the transition from chair to skew-boat significantly modified all the selected geometrical parameters: the C1−O6 bond is 0.015 Å shorter and the C1−O1 bond is 0.021 Å longer in the skew-boat conformation than in the chair conformation. The transition to the skew-boat decreased the O1−O4 distance by 1.110 Å or 20.6%. The only experimental value available of 0% was obtained for cellulose by AFM studies and is consistent with our results: the stretching force compensated the reduction in distance.

5. Discussion and Conclusions

The goal of this paper was to demonstrate how the chosen mathematical constraints enabled us to study the conformational

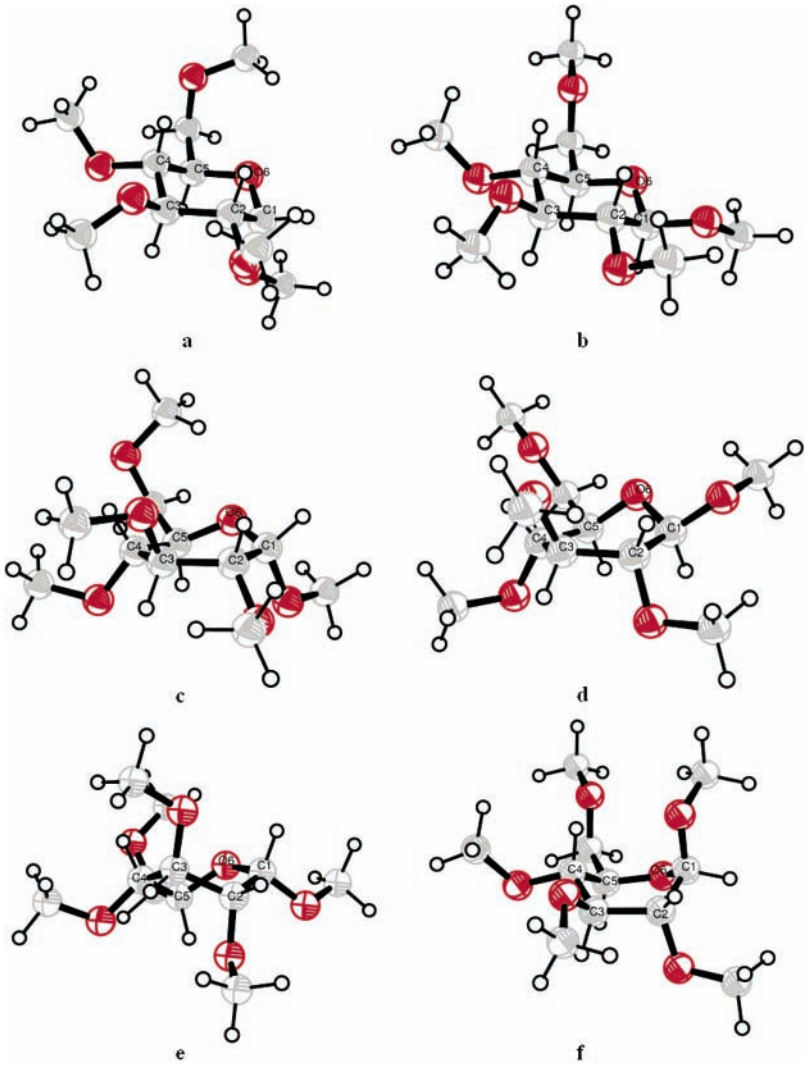

Figure 8. Stationary point geometries (ORTEP representation) for chair to skew-boat transitions of penta-*O*-methyl-α-D-glucopyranose (a) $^4C_1$, (c) ^OE, and (e) $^OS_2$ and penta-*O*-methyl-*β*-D-glucopyranose (b) $^4C_1$, (d) ^OE, and (f) $^OS_2$.

TABLE 5: Optimized Canonical Conformations for the Stationary Points on the Trajectory $^4C_1$ Chair to $^OS_2$ Skew-Boat for Penta-*O*-methyl-α- and Penta-*O*-methyl-*β*-D-glucopyranose

compd	canonical conformations
	Penta-*O*-methyl-α-D-glucopyranose
$^4C_1$	$^4C_1$, 0.935; $B_{2,5}$, 0.007; $^3S_1$, 0.074
^OE	^0E, 0.757; $^{O,3}B$, 0.046; $^1S_5$, 0.087
$^OS_2$	$^{1,4}B$, 0.181; $^4C_1$, 0.062; $^OS_2$, 1.009
	penta-*O*-methyl-*β*-D-glucopyranose
$^4C_1$	$^4C_1$, 0.926; $^{O,3}B$, 0.113; $^5S_1$, 0.005
^OE	^OE, 0.830; $^{O,3}B$, 0.253; $^1S_5$, 0.098
$^OS_2$	$^{1,4}B$, 0.801; $^OH_5$, 0.110; $^OS_2$, 0.850

transitions among selected pyranose conformations in both static and dynamical calculations. We have combined the constrained method with ab initio molecular dynamics calculations to sample the conformational space of glucopyranose and some model compounds. Our constrained method allowed us to define the chair, boat, skew-boat, half-chair, and envelope conformers and to map the low-energy paths connecting them.

The inversion process was conducted mainly via the q_1 constraint. The inversion trajectory passed through transition states situated on smaller radius circles halfway between the pseudorotational circle (the equator of the conformational sphere) and the two chairs (the poles of the conformational sphere). The inversion trajectory also evidenced a secondary minimum (usually a skew-boat) situated on the pseudorotational itinerary.

The internal coordinates q_2 and q_3 are equivalent and can be used to describe conformational change along the pseudorotational itinerary. We only simulated the pseudorotation along the equatorial itinerary for cyclohexane. The results showed that the trajectory followed the surface of the sphere and remained constrained to the pseudorotational itinerary; the skew-boat minima were interconnected along the inversion pathway by boat transition states. The energy barriers along the pseudorotational itinerary were about 4 kJ·mol^{-1}, in good agreement with experimental data.

We have also studied 2-oxanol, which is the simplest model for glucopyranose, as well as the α and *β* conformers of penta-*O*-methyl-D-glucopyranose. For 2-oxanol, we have highlighted a different trajectory than previously calculated. This inversion trajectory, passing through the ^2S_O conformer, was confirmed to be the lowest-energy pathway by static ab initio calculations.

For α- and *β*-D-glucopyranose, the calculations provided additional insights into the behavior of these anomers. We calculated for the first time a complete inversion trajectory for the D-glucopyranose system. The calculations indicated that a variety of structures were isoenergetic, suggesting a flat potential energy surface around the skew-boat secondary minima. Ac-

cording to our calculations, the free-energy barriers for the chair to twist-boat transition in α- and β-D-glucopyranose were 52 and 37 kJ·mol^{-1} (Table 4), respectively. These values can be compared to the ab initio constrained calculations of O'Donoghue et al.,[66] which gave a barrier height for the α-D-glucopyranose chair to twist-boat transition of about 59 kJ·mol^{-1} and gave a barrier height for the β-D-glucopyranose chair to boat transition of about 53 kJ·mol^{-1}. These values are internal energies and not free-energy differences and were obtained by a limited conformational search with only one of the three puckering coordinates constrained. Previous MM3 molecular mechanics studies also found a barrier of 50 kJ·mol^{-1} for the α-D-glucopyranose chair to twist-boat transition.[70] AFM studies suggested that the elastic properties of polyssacharides result from a force-induced elongation of the ring structure and a final transition from a chairlike to a boatlike conformation.[9] In contrast to these findings are the most recent AFM experiments, suggesting a mechanism involving relatively low-energy transition barriers for the chair extension, with the dominating process being an anti−syn isomerization of the dihedral angles for the α(1→4) linkage.[71]

In all of the above MD simulations, the system was thermostated at 300 K and the masses were rescaled. For the test molecules, about 70 000 steps were performed for each simulation, or approximately 12 ps of real time, and for the two D-glucopyranoses, 90 000 steps were performed for each simulation, or approximately 15 ps of real time. Both forward and reverse scans were performed to test the rate of change of the reaction coordinate. For example, for 2-oxanol, the calculated hysteresis showed for the forward and reverse estimates of the inversion free-energy barrier a difference of 5.3 kJ·mol^{-1}. This error arises from the *slow-growth* simulation, which is a necessary compromise to limit the computational effort to a reasonable level. The comparison of experimental and calculated conversion barriers suggests that this error source is limiting the overall accuracy of the calculations. Furthermore, the stationary points for both forward and reverse scans occurred at the same value of the reaction coordinate. The constrained dynamic calculations we presented above provided us with a tool for finding the lowest-energy pathway for the chair inversion of pyranoses and for calculating the inversion free-energy barrier by means of thermodynamic integration. We have complemented the dynamic simulation by static simulations.

Static simulations were used, first, to validate the free-energy results produced by our constrained dynamics method and, second, to access other thermodynamic properties such as the enthalpy of reaction, usually available from experimental data. Static calculations involved full optimization of reactants. Transition states were calculated by taking snapshots from the MD trajectory; no further optimization was done. Frequency calculations were performed on each of the stationary points.

The benchmark tests we have carried out on the enthalpy and the free-energy barrier of chair inversion of the six-membered saturated rings represented a remarkable agreement between experiment and theory for both quantities. For example, the lowering of the enthalpic barrier to inversion by oxygen substitution on going from cyclohexane to tetrahydropyran as well as the small difference in free energy were well reproduced by calculations.

Our constrained method was based on Car−Parrinello (CP) simulations. We emphasize that, although the CP method involves quantum mechanical calculations to determine the electronic structure, the actual dynamic is purely classical; therefore, quantum effects such as zero-point energy correction are not accounted for. However, the mean absolute deviation between MD and static simulations was 4.8 kJ·mol^{-1} for the model molecules; as for D-glucopyranoses, the MD simulations in both cases underestimated the free-energy barriers. We explained this, first, by additional steric and electronic effects not present with the model molecules and, second, by the mixed-inversion pseudorotation process that characterized the MD trajectories of D-glucopyranoses.

These results clearly demonstrate that our constrained method was able, first, to simulate accurate trajectories for the chair inversion of several pyranose conformations and, second, to calculate free-energy barriers that were in excellent agreement with both established static calculations and experimental data.

We consider these results a major step toward understanding the role of conformation change in the kinetic stability of sugar residues involved in glycosylation reactions. Our constrained method was successfully used to characterize the conformational potential energy surface by mapping important stationary points.

Acknowledgment. This work was partly supported by the iHPC multiscale modeling initiative of the NRC. This is NRC paper # 42504.

References and Notes

(1) Kochetkov, N. K. *Stud. Nat. Prod. Chem.* **1994**, *14*, 201−266.
(2) Sinnott, M. L. *Chem. Rev.* **1990**, *90*, 1171−1202.
(3) Horenstein, B. A.; Bruner, M. *J. Am. Chem. Soc.* **1998**, *120*, 1357−1362.
(4) Murray, B. W.; Wittmann, V.; Burkart, M. D.; Hung, S.-C.; Wong, C.-H. *Biochemistry* **1997**, *36*, 823−831.
(5) Deslongchamps, P.; Dory, Y. L.; Li, S. *Can. J. Chem.* **1994**, *72*, 2021−2027.
(6) Zhu, J.; Bennet, A. J. *J. Am. Chem. Soc.* **1998**, *120*, 3887−3893.
(7) Smith, B. J. *J. Am. Chem. Soc.* **1997**, *119*, 2699−2706.
(8) Liras, J.; Anslyn, E. In *Molecular Design and Bioorganic Catalysis;* Wilcox, C. S., Hamilton, A. D., Eds.; Kluwer Academic Publishing: The Netherlands, 1996.
(9) Marszalek, P. E.; Oberhauser, A. F.; Pang, Y. P.; Fernandes, J. M. *Nature* **1998**, *396*, 661−664.
(10) Nukada, T.; Bérces, A.; Zgierski, M. Z.; Whitfield, D. M. *J. Am. Chem. Soc.* **1998**, *120*, 13291−13295.
(11) Bérces, A.; Whitfield, D. M.; Nukada, T.; do Santos, Z. I.; Obuchowska, A.; Krepinsky, J. J. *Can. J. Chem.* **2004**, *82*, 1157−1171.
(12) Nukada, T.; Bérces, A.; Whitfield, D. M. *Carbohydr. Res.* **2002**, *337*, 765−774.
(13) Nukada, T.; Bérces, A.; Wang, L.; Zgierski, M. Z.; Whitfield, D. M. *Carbohydr. Res.* **2005**, *340*, 841−852.
(14) Stoddart, J. F. *Stereochemistry of Carbohydrates*; Wiley-Interscience: New York, 1971.
(15) Lichtenthaler, F. W.; Rönninger, S.; Lindner, H. J.; Immel, S.; Cuny, E. *Carbohydr. Res.* **1993**, *249*, 305−326.
(16) Dixon, D. A.; Komornicki, A. *J. Phys. Chem.* **1990**, *94*, 5630−5636.
(17) Bérces, A.; Whitfield, D. M.; Nukada, T. *Tetrahedron* **2001**, 477−491.
(18) Hendrickson, J. B. *J. Am. Chem. Soc.* **1967**, *89*, 7047−7061.
(19) Cremer, D.; Pople, J. A. *J. Am. Chem. Soc.* **1975**, *97*, 1354−1358.
(20) Haasnoot, C. A. G. *J. Am. Chem. Soc.* **1992**, *114*, 882−887.
(21) Zefirov, N.; Palyulin, V. A.; Dashevskaya, E. E. *J. Phys. Org. Chem.* **1990**, *3*, 147−158.
(22) Fogarasi, G.; Zhou, X.; Taylor, P. W.; Pulay, P. *J. Am. Chem. Soc.* **1992**, *114*, 8191−8201.
(23) Pulay, P.; Fogarasi, G.; Pang, F.; Boggs, J. E. *J. Am. Chem. Soc.* **1979**, *101*, 2550−2560.
(24) Blöchl, P. E. *Phys. Rev. B* **1994**, *50*, 17953−17979.
(25) Car, R.; Parrinello, M. *Phys. Rev. Lett.* **1985**, *55*, 2471−2474.
(26) Perdew, J. P.; Zunger, A. *Phys. Rev. B* **1981**, *23*, 5048−5079.
(27) Blöchl, P. E. *J. Chem. Phys.* **1995**, *103*, 7422−7428.
(28) Hoover, W. G. *Phys. Rev. A* **1985**, *31*, 1695−1697.
(29) Nose, S. *Mol. Phys.* **1984**, *52*, 255−268.
(30) Blöchl, P. E.; Parrinello, M. *Phys. Rev. B* **1992**, *45*, 9413−9416.
(31) Ryckaert, J. P.; Ciccotti, G.; Berendsen, H. J. C. *J. Comput. Phys.* **1977**, *23*, 327−341.
(32) Margl, P. M.; Ziegler, T.; Blöchl, P. E. *J. Am. Chem. Soc.* **1995**, *117*, 12625−12634.

(33) Margl, P. M.; Lohrenz, J. C. W.; Ziegler, T.; Blöchl, P. E. *J. Am. Chem. Soc.* **1996**, *118*, 4434−4441.
(34) Margl, P. M.; Ziegler, T.; Blöchl, P. E. *J. Am. Chem. Soc.* **1996**, *118*, 5412−5419.
(35) Yang, S.-Y.; Hristov, I.; Fleurat-Lessard, P.; Ziegler, T. *J. Phys. Chem. A* **2005**, *109*, 197−204.
(36) Frisch, M. J.; Trucks, G. W.; Schlegel, H. B.; Scuseria, G. E.; Robb, M. A.; Cheeseman, J. R.; Zakrzewski, V. G.; Montgomery, J. A., Jr.; Stratmann, R. E.; Burant, J. C.; Dapprich, S.; Millam, J. M.; Daniels, A. D.; Kudin, K. N.; Strain, M. C.; Farkas, O.; Tomasi, J.; Barone, V.; Cossi, M.; Cammi, R.; Mennucci, B.; Pomelli, C.; Adamo, C.; Clifford, S.; Ochterski, J.; Petersson, G. A.; Ayala, P. Y.; Cui, Q.; Morokuma, K.; Malick, D. K.; Rabuck, A. D.; Raghavachari, K.; Foresman, J. B.; Cioslowski, J.; Ortiz, J. V.; Stefanov, B. B.; Liu, G.; Liashenko, A.; Piskorz, P.; Komaromi, I.; Gomperts, R.; Martin, R. L.; Fox, D. J.; Keith, T.; Al-Laham, M. A.; Peng, C. Y.; Nanayakkara, A.; Gonzalez, C.; Challacombe, M.; Gill, P. M. W.; Johnson, B. G.; Chen, W.; Wong, M. W.; Andres, J. L.; Head-Gordon, M.; Replogle, E. S.; Pople, J. A. *Gaussian 98*, revision A.11.3; Gaussian, Inc.: Pittsburgh, PA, 1998.
(37) Becke, A. D. *Phys. Rev. A* **1988**, *38*, 3098−3100.
(38) Perdew, J. P. *Phys. Rev. B* **1986**, *33*, 8822−8824.
(39) Perdew, J. P. *Phys. Rev. B* **1986**, *34*, 7406.
(40) Ross, B. D.; True, N. S. *J. Am. Chem. Soc.* **1983**, *105*, 1382.
(41) Pickett, H. M.; Strauss, H. L. *J. Am. Chem. Soc.* **1970**, *92*, 7281.
(42) Squillacote, M.; Sheridan, R. S.; Chapman, O. L.; Anet, F. A. L. *J. Am. Chem. Soc.* **1975**, *97*, 3244−3246.
(43) del Carmen Fernández-Alonso, M.; Asensio, J. L.; Cañada, F. J.; Jiménez-Barbero, J.; Cuevas, G. *ChemPhysChem* **2003**, *4*, 754−757.
(44) Cramer, C. J.; Truhlar, D. G. *J. Am. Chem. Soc.* **1993**, *115*, 5745−5753.
(45) Joshi, N.; Rao, V. *Biopolymers* **1979**, *18*, 2993−3004.
(46) Tvaroska, I.; Kozar, T. *J. Am. Chem. Soc.* **1980**, *102*, 6929−6936.
(47) Back, D.; Polavarapu, P. *J. Comput. Chem.* **1987**, *8*, 772−777.
(48) Woods, R.; Szarek, W.; Smith, V. *J. Chem. Soc., Chem. Commun.* **1991**, *5*, 334−337.
(49) McNamara, J. P.; Muslim, A.-M.; Abdel-Aal, H.; Wang, H.; Mohr, M.; Hillier, I. H.; Bryce, R. A. *Chem. Phys. Lett.* **2004**, *394*, 429−436.
(50) Jeffrey, G.; Taylor, R. *J. Comput. Chem.* **1980**, *1*, 99−109.
(51) Rasmussen, K. *Acta Chem. Scand., Ser. A* **1982**, *36*, 323−327.
(52) Dowd, M.; Reilly, P.; French, A. *J. Comput. Chem.* **1992**, *13*, 102−114.
(53) Jeffrey, G. A.; Pople, J. A.; Binkley, J. S.; Vishveshwara, S. *J. Am. Chem. Soc.* **1978**, *100*, 373−379.
(54) Melberg, S.; Rasmussen, K.; Scordamaglia, R.; Tosi, C. *Carbohydr. Res.* **1979**, *76*, 23−37.
(55) French, A.; Schfer, L.; Newton, S. *Carbohydr. Res.* **1993**, *239*, 51−60.
(56) Appell, M.; Strati, G.; Willett, J. L.; Momany, F. A. *Carbohydr. Res.* **2004**, *339*, 537−551.
(57) Momany, F. A.; Appell, M.; Strati, G.; Willett, J. L. *Carbohydr. Res.* **2004**, *339*, 553−567.
(58) Rees, D. A.; Smith, P. J. C. *Perkin Trans.* **1975**, *2*, 830−835.
(59) Rees, D. A.; Smith, P. J. C. *Perkin Trans.* **1975**, *2*, 836−840.
(60) Peters, T.; Meyer, B.; Stuike-Prill, R.; Somorjai, R.; Brisson, J.-R. *Carbohydr. Res.* **1993**, *238*, 49−73.
(61) Brady, J. W. *J. Am. Chem. Soc.* **1986**, *108*, 8153−8160.
(62) Brady, J. W. *J. Am. Chem. Soc.* **1989**, *111*, 5155−5165.
(63) Ha, S.; Gao, J.; Tidor, B.; Brady, J. W.; Karplus, M. *J. Am. Chem. Soc.* **1991**, *113*, 1553−1557.
(64) O'Donoghue, P.; Luthey-Schulten, Z. A. *J. Phys. Chem. B* **2000**, *104*, 10398−10405.
(65) Chen, J. Y.-J.; Naidoo, K. J. *J. Phys. Chem. B* **2003**, *107*, 9558−9566.
(66) Marszalek, P. E.; Pang, Y.-P.; Li, H.; Yazal, J. E.; Oberhauser, A. F.; Fernandez, J. M. *Proc. Natl. Acad. Sci. U.S.A.* **1999**, *96*, 7894−7898.
(67) (a) Barrows, S.; Dulles, F.; Cramer, C.; French, A.; Truhlar, D. *Carbohydr. Res.* **1995**, *276*, 219−251. (b) Whitfield, D. M. *J. Mol. Struct.: THEOCHEM* **1997**, *395*, 53−59. (c) Polavarapu, P. L.; Ewig, C. S. *J. Comput. Chem.* **1992**, *13*, 1255. (d) Jeffrey, G. A. *J. Mol. Struct.* **1990**, *237*, 75−79.
(68) Mendonca, A.; Johnson, G.; French, A.; Laine, R. *J. Phys. Chem. A* **2002**, *106*, 4115−4124.
(69) Anderson, J. E.; Ijeh, A. I. *J. Chem. Soc., Perkin Trans. 2* **1994**, *9*, 1965−1968.
(70) Dowd, M. K.; French, A. D.; Reilly, P. J. *J. Comput. Chem.* **1994**, *264*, 1−19.
(71) Kuttel, M.; Naidoo, K. J. *J. Am. Chem. Soc.* **2005**, *127*, 12−13.